The Partially Folded Homodimeric Intermediate of *Escherichia coli* Aspartate Aminotransferase Contains a "Molten Interface" Structure[†]

Edgar Deu, Jashdeep Dhoot, and Jack F. Kirsch*

Department of Molecular and Cell Biology, University of California, Berkeley, California 94720-3206

Received July 30, 2008; Revised Manuscript Received October 27, 2008

ABSTRACT: The role of intersubunit side chain−side chain interactions in the stability of the *Escherichia coli* aspartate aminotransferase (eAATase) homodimer was investigated by directed mutagenesis at 10 different interface contacts. The urea-mediated unfolding pathway of this enzyme proceeds through the formation of a dimeric intermediate, D*, that retains only 40% of the native enzyme secondary structure as judged by circular dichroism. Disruption of any single intersubunit interaction results in a >2.6 kcal mol^{-1} decrease in native state stability, independent of its location or nature. However, the stability of D* with respect to U, the unfolded monomer, is the same for all mutants. The stability of the eAATase interface cannot be ascribed to the contribution of a few hot spots, or to the accumulation of a large number of weak interactions, but only to the presence of multiple important and interconnected interactions. It is proposed that a "molten interface" structure, flexible enough to accommodate point mutations, accounts for the stability of D*. Nuclei of tertiary structure, which are not involved in native intersubunit contacts, likely provide a scaffold for the unstructured interface of D*. Such a scaffold would account for the cooperative unfolding of the intermediate.

Protein function can be fully understood only within the context of interaction with other proteins and with other components of the biological environment. Knowledge of the composition, formation, stability, and structural organization of protein−protein interfaces is crucial in the acquisition of a functional understanding of any participatory biological process. While the thermodynamics and kinetics of formation of a number of protein−protein complexes have been thoroughly investigated, typical examples being barnase−barstar (*3*−*6*), antigen−antibody (*7*−*10*), or protein ligand−receptor complexes (*11*−*14*), comparatively few studies have been performed on obligate multimeric proteins. The latter systems differ from the former systems in that the individual polypeptide chains of such assemblies generally do not exist as folded monomeric entities under physiological conditions, and therefore, the oligomers are likely formed during or immediately following translation. The thermodynamic characterization of obligate multimers may be understood only within the context of protein folding.

Despite the predominance of large oligomeric proteins in living organisms, most folding studies have been performed on globular or small multidomain monomers and mainly report on their secondary and tertiary structural organization. There have been comparatively few detailed thermodynamic investigations of large multimeric proteins (*15*−*18*), and thorough characterization of obligate multimer interfaces by site-directed mutagenesis has been restricted to very small systems such as coil−coil formation (*19*), the tumor repressor p53 tetramerization domain (*20*), or the 10 kDa P22 Arc repressor homodimer (*21*). Although it is generally accepted that the organization and properties of obligate multimer interfaces should be similar to those of interdomain contact regions found in monomeric proteins (*22*), few thermodynamic data for testing those hypotheses are available.

Escherichia coli aspartate aminotransferase (eAATase)[1] is a relatively large homodimeric protein (87 kDa) whose stability has been well characterized (*1, 2, 23*−*27*). Each monomer is composed of an N-terminal (Nt) tail (residues 5−15) (*28*), a large domain (residues 47−329), and a small domain (residues 16−46 and 330−409). (The numbering of residues is based on the *Pig* cytosolic AATase sequence.) Its >3000 $Å^2$ broad interface is composed of a large contact area between the two large domains and of two equivalent smaller surfaces formed by the Nt tails that wrap around the opposite large domains (Figure 1). The former interface is composed mainly of electrostatic and hydrogen bond interactions, while the intersubunit side chain contacts in the latter are predominantly nonpolar.

The two pyridoxal 5′-phosphate (PLP)-dependent active sites are nested at the inter-large domain interface. The enzyme catalyzes the reversible transfer of an amino group from an acidic amino acid to a dicarboxylic α-keto acid (eq 1).

[†] This work was supported NIH Grant GM 35393.

* To whom correspondence should be addressed. Telephone: (510) 642-6368. E-mail: jfkirsch@berkeley.edu.

[1] Abbreviations: ΔASA, change in solvent accessible area; σ, standard deviation; C_m, denaturant concentration at a transition midpoint; D, folded homodimeric state; D*, partially unfolded homodimeric intermediate; DTT, dithiothreitol; eAATase, *E. coli* aspartate aminotransferase; His_6 tag, six-histidine tag; I, unfolding intermediate species; KEEK, K68E/E265K double mutant; KMEQ, K68M/E265Q double mutant; KG, α-ketoglutarate; LEM, linear extrapolation method; *m*, cooperativity parameter; N, native state; Nt, N-terminal; PCR, polymerase chain reaction; PLP, pyridoxal 5′-phosphate; P_T, total concentration of monomer; U, unfolded state; WT, wild type; X_{D*}, mole fraction of D*.

10.1021/bi801431x CCC: $40.75
Published on Web 12/19/2008

L-aspartate + α-ketoglutarate (KG) ⇄ oxaloacetate + L-glutamate (1)

The ping-pong mechanism of this enzyme has been investigated in depth (*29*−*32*), and the catalytic roles of several residues involved in quaternary interactions have been characterized (*33*−*37*).

eAATase unfolds in the presence of urea through a dimeric intermediate (D*) (eq 2) that retains <50% of the native secondary structure. The active site regions of D* are unstructured and do not bind PLP (*1, 2*).

$$\text{D-PLP}_2 \rightleftarrows 2\text{PLP} + \text{D}^* \rightleftarrows 2\text{U} \quad (2)$$

where D-PLP_2 is the native PLP-bound homodimer and U the unfolded monomer. The total free energy of unfolding of the apoenzyme is 36 ± 3 kcal mol^{-1} (*1*), and PLP stabilizes D by ∼6 kcal mol^{-1} (*2*) (both values are given for a 1 M standard state). Despite the significant structural losses undergone in the D ⇄ D* transition, this intermediate is quite stable ($\Delta G^0_{D^*\rightleftarrows 2U}$ = 25 ± 1 kcal mol^{-1}), unfolds cooperatively ($m_{D^*\rightleftarrows 2U}$ = 3.4 ± 0.2 kcal mol^{-1} M^{-1}), and persists as a dimer at urea concentrations of ≤5.3 M. It was proposed that the D* quaternary interactions, which might also be the key intersubunit contacts in D, must be located in a dimerization region removed from the active sites (*2*).

It is of special interest to understand how the large and small interfaces of this enzyme and their amino acid compositions contribute to the stability of the native (D) and partially folded intermediate (D*) species. The intersubunit location of the active sites implies that the interface structure is vital for the catalytic function of this enzyme. However, the extent to which catalytically important intersubunit residues contribute to dimer stability is unknown. Hydrophobic and electrostatic side chain−side chain interactions distributed throughout the eAATase interface were perturbed by site-directed mutagenesis to address those questions.

MATERIALS AND METHODS

Site-Directed Mutagenesis and Purification of eAATase Variants. All mutants contain a C-terminal six-histidine tag (His_6 tag) (*33*) and were made by PCR. Cloning of His_6-tagged wild-type eAATase (WT) into the pBluescriptII KS+ (Stratagene) plasmid (pKS+AAT) and site-directed mutagenesis at positions 68 and 265 (pKS+K68M, pKS+K68E, pKS+E265Q, pKS+E265K, pKS+KMEQ, and pKS+KEEK) are described in ref *33*. The same procedure was used to obtain pKS+R266M, pKS+R266K, and pKS+N294D. Stratagene's Quick-Change protocol was followed for introduction of all the other mutations (pKS+F6A, pKS+E7A, pKS+I9A, pKS+T10A, pKS+D15A, pKS+N294R, and pKS+N297R), except that the PCR extension time was doubled. Expression and purification of holoenzymes were performed as reported previously (*1, 2, 33*). The proteins were stored in 20 mM phosphate buffer containing 10 μM PLP at pH 7.5 and 4 °C.

Denaturation of eAATase Variants. Concentrations of holoenzyme of 0.5−10 μM (all protein concentrations given as monomer concentrations) were incubated overnight in 20 mM potassium phosphate, 1 mM DTT, 10 μM PLP, and 0−8 M urea at pH 7.5 and 25 °C (*1, 2*). Urea concentrations were based on the refractive index (*38, 39*). The extent of protein unfolding was measured by monitoring the changes in tryptophan fluorescence at 335 nm (λ_{ex} = 280 nm). Emission spectra of the native, partially folded, and unfolded states were recorded between 300 and 400 nm for each mutant. The dimer dissociation process was generally identified by comparing denaturation curves obtained as functions of enzyme concentration. The buffer signals were linearly dependent on urea concentration and were subtracted from the data prior to further analysis. All measurements were recorded at 25 °C on a PerkinElmer LB50S fluorimeter.

Data Analysis. (A) Transition Midpoints. For each enzyme concentration, the fluorescence data were fitted to a three-state unimolecular denaturation model (eq 3) with eq 4 (*1, 40, 41*).

$$\text{N}\rightleftarrows\text{I}\rightleftarrows\text{U} \quad (3)$$

$$S = [S_N^0 + \alpha_N[\text{urea}] + (S_I^0 + \alpha_I[\text{urea}])K_{N\rightleftarrows I} + (S_U^0 + \alpha_U[\text{urea}])K_{N\rightleftarrows I}K_{I\rightleftarrows U}]/[1 + K_{N\rightleftarrows I}(1 + K_{I\rightleftarrows U})] \quad (4)$$

where N, I, and U are the native, intermediate, and unfolded states, respectively, S is the measured fluorescence, S_i^0 the intrinsic fluorescence of species i at 0 M urea, and α_i the dependence of the intrinsic fluorescence of species i on denaturant concentration. $K_{N\rightleftarrows I}$ and $K_{I\rightleftarrows U}$ are defined according to the linear extrapolation method (LEM) (*39, 42*) with eqs 5 and 6, respectively

$$K_{N\rightleftarrows I} = \exp[m_{N\rightleftarrows I}([\text{urea}] - C_{m,N\rightleftarrows I})/RT] \quad (5)$$

$$K_{I\rightleftarrows U} = \exp[m_{I\rightleftarrows U}([\text{urea}] - C_{m,I\rightleftarrows U})/RT] \quad (6)$$

where m is the cooperativity parameter and C_m the urea concentration at the transition midpoint of the indexed equilibrium.

(B) Cooperativity Parameters. The observed transitions for all eAATase variants are consistent with the model of eq 2 (*1, 2*). The data densities in the transition regions for most mutants were insufficient to determine accurate m values; therefore, $m_{D\rightleftarrows D^*}$ and $m_{D^*\rightleftarrows 2U}$ were computed independently from a global fit of the experimental data using the LEM as outlined below.

Pre- and post-transition baselines calculated from eq 4 (S_i^0 and α_i parameters) were used to compute X_{D^*} (mole fraction of dimeric intermediate) during the formation (eq 7) and unfolding (eq 8) of D*.

$$X_{D^*} = \frac{S - (S_N^0 + \alpha_N[\text{urea}])}{(S_I^0 + \alpha_I[\text{urea}]) - (S_N^0 + \alpha_N[\text{urea}])}; \quad \text{for [urea] within the D} \rightleftarrows \text{D* transition} \quad (7)$$

$$X_{D^*} = \frac{S - (S_U^0 + \alpha_U[\text{urea}])}{(S_I^0 + \alpha_I[\text{urea}]) - (S_U^0 + \alpha_U[\text{urea}])}; \quad \text{for [urea] within the D*} \rightleftarrows \text{2U transition} \quad (8)$$

Free energy changes associated with each equilibrium transition were calculated according to eqs 9 and 10.

$$\Delta G_{D\rightleftarrows D^*} = -RT\ln(K_{D\rightleftarrows D^*}) = -RT\ln[X_{D^*}/(1 - X_{D^*})]; \quad 0.1 < X_{D^*} < 0.9 \quad (9)$$

$$\Delta G_{D^*\rightleftarrows 2U} = -RT\ln(K_{D^*\rightleftarrows 2U}) = -RT\ln\{[2P_T(1 - X_{D^*})^2]/X_{D^*}\}; 0.1 < X_{D^*} < 0.9 \quad (10)$$

Equations 7−10 are fully described in ref *1*; P_T is the total concentration of monomer. X_{D^*} values outside the indicated

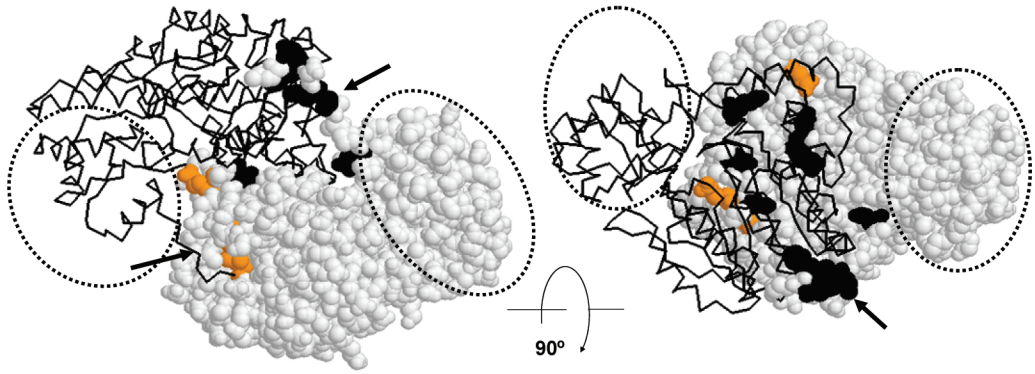

FIGURE 1: Map of mutated interface residues in the eAATase structure. One monomer is represented with a space-filling model and the other with its backbone thread to highlight the homodimer interface. Arrows and dotted circles indicate the positions of the Nt tails and small domains, respectively. The latter are not involved in intersubunit interactions. Intersubunit amino acids targeted for mutagenesis are colored black. Orange residues were not altered but directly interact with mutated positions in the opposite subunit.

range could not be determined accurately and were not used in the following calculations.

The LEM formula (eq 11) was rewritten (eq 12) by centering each transition midpoint at 0 M urea ($[\text{urea}]_{\text{Corr}} = [\text{urea}] - C_m$) and used to compute $m_{D\rightleftarrows D^*}$ and $m_{D^*\rightleftarrows 2U}$ independently.

$$\Delta G = \Delta G^0 - m[\text{urea}] \quad (11)$$

$$\Delta G = \Delta G^{C_m} - m[\text{urea}]_{\text{Corr}} \quad (12)$$

where ΔG^{C_m} is the free energy change associated with the measured process at the transition midpoint. For the D $\rightleftarrows$ D* equilibrium, $\Delta G^{C_m}{}_{D\rightleftarrows D^*} = 0$ (eq 9 with $X_{D^*} = 0.5$), and $m_{D\rightleftarrows D^*}$ is obtained from a fit of all calculated $\Delta G_{D\rightleftarrows D^*}$ values (eq 9) to eq 13.

$$\Delta G_{D\rightleftarrows D^*} = A - m_{D\rightleftarrows D^*}[\text{urea}]_{\text{Corr}} \quad (13)$$

For the D* $\rightleftarrows$ 2U equilibrium, $\Delta G^{C_m}{}_{D^*\rightleftarrows 2U} = -RT \ln P_T$ (eq 10 with $X_{D^*} = 0.5$). Thus, $m_{D^*\rightleftarrows 2U}$ can be obtained from the slope of eq 14.

$$\Delta G_{D^*\rightleftarrows 2U} + RT \ln P_T = A - m_{D^*\rightleftarrows 2U}[\text{urea}]_{\text{Corr}} \quad (14)$$

$\Delta G_{D^*\rightleftarrows 2U}$ values are computed with eq 10. Theoretically, eqs 13 and 14 should intercept at the origin ($A = 0$).

(C) ΔG^0 Values. The denaturation data were treated according to the model of eq 2. For each mutant concentration, X_{D^*} values obtained from eqs 7 and 8 were fitted to eq 15 (*1, 16, 18, 43*), where the *m* parameters were fixed to the globally fitted values.

$$X_{D^*} = K_{D\rightleftarrows D^*}\{4P_T(1 + K_{D\rightleftarrows D^*}) + K_{D\rightleftarrows D^*}K_{D^*\rightleftarrows 2U} - [(K_{D\rightleftarrows D^*}K_{D^*\rightleftarrows 2U})^2 + 8P_T K_{D\rightleftarrows D^*}K_{D^*\rightleftarrows 2U}(1 + K_{D\rightleftarrows D^*})]^{1/2}\}/[4P_T(1 + K_{D\rightleftarrows D^*})] \quad (15)$$

where $K_{D\rightleftarrows D^*} = \exp[-(\Delta G^0{}_{D\rightleftarrows D^*} - m_{D\rightleftarrows D^*}[\text{urea}])/RT]$, and $K_{D^*\rightleftarrows 2U} = \exp[-(\Delta G^0{}_{D^*\rightleftarrows 2U} - m_{D^*\rightleftarrows 2U}[\text{urea}])/RT]$. The errors associated with the ΔG^0 values ($\sigma_{\Delta G^0}$) were estimated from eq 16 (*44*).

$$\sigma_{\Delta G^0} = \sqrt{\sigma_m{}^2 C_m{}^2 + \sigma_{C_m}{}^2 m^2} \quad (16)$$

where σ_m and σ_{C_m} are the standard deviations associated with those parameters. The effect of interface mutations on the stability of eAATase is quantified by eq 17

$$\Delta\Delta G^0{}_{(\text{Mutant})} = \Delta G^0{}_{(\text{Mutant})} - \Delta G^0{}_{(\text{WT})} \quad (17)$$

where $\Delta G^0{}_{(\text{Mutant})}$ is the average of independently determined $\Delta G^0{}_{D\rightleftarrows D^*}$ or $\Delta G^0{}_{D^*\rightleftarrows 2U}$ values at varied enzyme concentrations. $\Delta G^0{}_{(\text{WT})}$ was calculated by fitting all the denaturation data reported for PLP-bound eAATase (*2*) to eq 15 with the *m* values calculated here. Double mutant cycles were carried out as described previously (*33, 45*−*47*).

RESULTS

Selection and Perturbation of Potentially Important Interactions at the eAATase Interface. Intersubunit contacts are defined by the crystal structure of PLP-bound eAATase [PDB entry 1ASN (*28*)] with a 4 Å cutoff. Only side chain−side chain interactions were considered for site-directed mutagenesis. Those judged to be potentially important for the interface stability are listed in Table 1 along with the point mutations designed to disrupt them. Three intersubunit interactions (Lys68−Glu265*, Arg266−Asn297*, and Asn294−Asn294*) spaced >8 Å from each other were chosen to map the stability contribution at different locations of the large domain−large domain interface. (Asterisks indicate residues from the opposite subunit.) Most of the targeted amino acids were replaced with both a relatively conservative substitution and a more disruptive replacement (K68M and K68E, E265Q and E265K, R266K and R266M, and N294D and N294R) to provide a better understanding of the forces that contribute to the interface stability at each position. N297D and double mutants K68M/E265Q (KMEQ) and K68E/E265K (KEEK) were also constructed.

Selected Nt tail residues involved in intersubunit interactions were substituted with alanine (F6A, I9A, T10A, and D15A). Additionally, the interactions of the Glu7 carboxylate group with the N-terminal amino group of Met5 and the Phe6 peptidic NH were disrupted (E7A) to investigate the importance of the Nt tail internal structure in mediating interface contacts. Interactions targeted for mutagenesis are mapped in Figure 1.

All Interface Mutants Unfold through the Same D Intermediate.* Urea-mediated unfolding of eAATase variants was monitored by fluorescence (λ_{ex} = 280 nm; λ_{em} = 335 nm). All denaturation curves show the same trend as those obtained for WT, i.e., an ~5-fold increase in emission intensity at intermediate denaturant concentrations followed by an ~2.5-fold decrease at higher urea concentrations (Figure 2). The former emission change is mainly due to

Table 1: Potential Important Intersubunit Interaction Contributors to eAATase Homodimer Stability[a]

	interaction	type	disruptive mutations
inter-large domain interface	Val39−Tyr70*	hydrophobic	
	Glu57−Lys68*	salt bridge[b]	K68M, K68M/E265Q, K68E, and K68E/E265K
	Lys68−Glu265*	salt bridge[b]	K68M, E265Q, K68M/E265Q, K68E, E265K, and K68E/E265K
	Asn69−Asn264*	H-bond	
	R113−R113*	H-bond	
	R113−D117*	salt bridge	
	Arg266−Asn297*	H-bond[b]	R266K, R266M, N297R
	Asn294−Asn294*	H-bond[b]	N294D, N294R
	His301−His301*	stacking	
large domain−N-terminal tail interface	Met5−Val125*	hydrophobic	
	Phe6−Phe118*	hydrophobic[b]	F6A
	Phe6−Val272*	hydrophobic[b]	F6A
	Ile9−Phe118*	hydrophobic[b]	I9A
	Asp15−Arg292*	salt bridge[b]	D15A
intra-N-terminal tail	Glu7−Met5	H-bonds[b,c]	E7A

[a] Intersubunit side chain−side chain interactions were identified from the eAATase crystal structure with a 4 Å cutoff (*28*). Asterisks indicate residues from the second subunit. [b] Denotes interaction perturbed by mutagenesis in this work. [c] Met5 is the N-terminal amino acid. The γ-carboxylate group of Glu7 makes hydrogen bonds with both the amino terminus and the first peptide bond.

solvent exposure of Trp140 upon cofactor dissociation (*2, 48*). The emission spectra of the folded, intermediate, and unfolded species for each mutant are comparable to those observed for the WT enzyme (data not shown). Only the transition at higher denaturant concentrations is enzyme concentration-dependent (see the C_m values in Table 2 and the insets of Figure 2). These results indicate that all mutants unfold through the same partially folded dimeric intermediate, D* (eq 2). T10A and N294R stabilities were measured at a single enzyme concentration, but their denaturation curves present the above-mentioned characteristics; therefore, the same denaturation model was also assigned to these two mutants.

Interface mutations affect only the D ⇄ D* transition. The $C_{m,D\rightleftarrows D^*}$ values are 0−1.4 M urea lower than that of WT. In contrast, very little variation is observed in $C_{m,D^*\rightleftarrows 2U}$ at a given enzyme concentration (Table 2 and Figure 2). This is especially interesting since all mutations were designed to disrupt the homodimer interface.

Coupled Denaturation Transitions Decrease the Apparent Cooperativity of Unfolding. In general, changes in solvent accessible surface area (ΔASA) and *m* values associated with denaturation processes are considered to be proportional to each other (*49*). Ordinarily, a single point mutation would not significantly change the total ΔASA due to unfolding, especially for large proteins such as eAATase. Thus, average *m* values are commonly used to calculate free energies of unfolding and to compare the stabilities of different point mutants (*44*).

However, the LEM is likely to yield underestimated *m* values if more than two species exist in the transition region of a denaturation curve (*39*). Spudich and Marqusee identified a hidden partially folded intermediate from an unusually low apparent *m* value in an *E. coli* ribonuclease HI mutant (*50*). The denaturation transitions for several eAATase variants, including WT, exhibit coupling between D ⇄ D* and D* ⇄ 2U steps, especially at low enzyme concentrations. This indicates that D, D*, and U coexist at intermediate urea concentrations (*2*).

To examine how the coupling between the two denaturation steps affects the apparent *m* values, $m_{D\rightleftarrows D^*}$ and $m_{D^*\rightleftarrows 2U}$ were globally fitted by either including or excluding measurements obtained from denaturation conditions that resulted in overlapping transitions (Figure 3). Lower *m* values and poorer Pearson factors (R^2) are found when all of the data are included in the fit. The values obtained from uncoupled transition data ($m_{D\rightleftarrows D^*} = 4.6 \pm 0.2$ kcal mol^{-1} M^{-1}, and $m_{D^*\rightleftarrows 2U} = 3.5 \pm 0.3$ kcal mol^{-1} M^{-1}) are within experimental error of those reported for apo-eAATase ($m_{D\rightleftarrows D^*} = 4.8 \pm 0.8$ kcal mol^{-1} M^{-1}, and $m_{D^*\rightleftarrows 2U} = 3.4 \pm 0.2$ kcal mol^{-1} M^{-1}) (*1*) and were used in eq 15 to calculate $\Delta G^0_{D\rightleftarrows D^*}$ and $\Delta G^0_{D^*\rightleftarrows 2U}$ (Table 2).

Effect of Interface Mutations on Stability. Any homodimer mutation perturbs two identical sites. Thus, the $\Delta\Delta G^0$ values reported in Figure 4 reflect the disruption of two equivalent but spatially distant interactions, except for position 294 where Asn294 interacts with Asn294* of the opposite subunit (Table 1). Fourteen of the 16 mutants (all but N294D and T10A) perturb the stability of the native state ($\Delta\Delta G^0_{D\rightleftarrows D^*}$) by 2.6 ± 0.2 to 7.3 ± 0.2 kcal mol^{-1} (Table 2 and Figure 4). Therefore, the vast majority of the interface residues chosen for mutagenic analysis are involved in interactions that are important for the stability of eAATase. However, none of them significantly affects the stability of the D* intermediate relative to U; all $\Delta\Delta G^0_{D^*\rightleftarrows 2U} \sim 0$ kcal mol^{-1} (see Figure 4).

Local Perturbations at the Large Domain−Large Domain Interface. (A) Lys68−Glu265 Intersubunit Salt Bridge.* Lys68 participates in two salt bridge interactions across the interface with Glu265* and Glu57*. Burial of three negative charges at this site strongly destabilizes the enzyme ($\Delta G^0_{D\rightleftarrows D^*(K68E)} = -4.8 \pm 0.2$ kcal mol^{-1}), but it is not the most detrimental mutation at this locus. A positive charge at position 265 (E265K or KEEK) destabilizes the enzyme by $>6.5 \pm 0.2$ kcal mol^{-1} (part of this effect is probably due to steric clashes of the large E265K* side chain with Lys68, Pro299, Ala300, His301, or Asn264*). Enhancing the effect of the Glu265* negative charge via the K68E or K68M mutation is less detrimental than neutralizing it (E265Q). Thus, the negative charge of Glu265* is a stronger contributor to stability than the positive charge at position 68 (K68M, K68E, and KMEQ are equally stable).

This contrasts with the role of this salt bridge in the activity of eAATase (*33*). Mutations at position 68, especially K68E, were found to impair the enzyme catalytically much more strongly than replacements of Glu265* (e.g., 100- and 10-

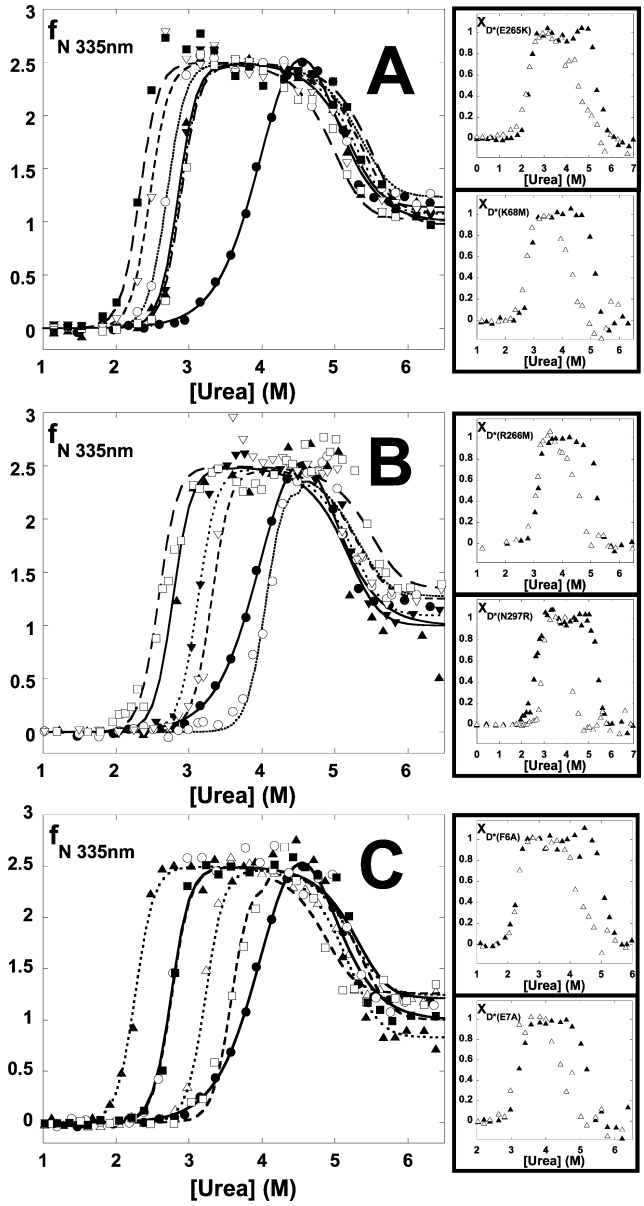

FIGURE 2: Fluorescence as a function of urea concentration for interface mutants. Holoenzyme samples were incubated overnight at 25 °C in 0−8 M urea and 10 μM PLP. Tryptophan emission at 335 nm (λ_{ex} = 280 nm) was monitored during unfolding for the following eAATase variants. (A) Lys68−Glu265* salt bridge mutations: 5 μM WT (●), K68M (▲), E265Q (○), KMEQ (▼), K68E (□), E265K (■), and KEEK (▽). (B) Other large domain replacements: 5 μM WT (●) and 10 μM R266K (▲), R266M (▼), N294D (○), N294R (▽), and N297R (□). (C) Nt tail alanine scanning: 5 μM WT (●), F6A (▲), E7A (△), T10A (□), and D15A (■) and 10 μM I9A (○). The lines represent simulated fluorescence curves calculated from fitted ΔG^0 (Table 2) and m (Figure 3) values. Insets show the dependence of X_{D^*} on urea concentrations at high (▲) and low (△) enzyme concentrations for representative mutants.

fold decrease in $k_{cat}/K_{M,KG}$ for K68E and E265K, respectively). The dominant role of position 68 in activity and of residue 265 in stability might explain why this electrostatic interaction is conserved in 80% of family Iα aminotransferases. An interesting exception is the Met68−Gln265* pair conserved in plant mitochondrial AATases (*33*). The KMEQ mutant of eAATase is almost as active as WT (*33*) but significantly less stable (Figure 4). The latter effect might be compensated by a set of seven residues that were found

Table 2: Stability Parameters for eAATase Holoenzyme Mutants[a]

	[protein] (μM)	$C_{m,D\rightleftarrows D^*}$ (M)	$C_{m,D^*\rightleftarrows 2U}$ (M)	$\Delta\Delta G^0_{D\rightleftarrows D^*}$[b] (kcal mol^{-1})
WT	5	3.89 (0.04)	5.02 (0.03)	−
F6A	1	2.28 (0.02)	4.26 (0.07)	−7.3 (0.4)
	5	2.28 (0.02)	5.09 (0.03)	−7.4 (0.4)
E7A	1	3.04 (0.02)	4.5 (0.1)	−3.8 (0.5)
	5	3.20 (0.02)	5.03 (0.04)	−3.0 (0.6)
I9A	1	2.81 (0.01)	4.42 (0.04)	−4.9 (0.5)
	10	2.74 (0.02)	5.20 (0.03)	−5.1 (0.5)
T10A	5	3.62 (0.03)	4.77 (0.03)	−1.3 (0.6)
D15A	0.85	2.77 (0.07)	3.8 (0.4)	−5.8 (0.6)
	1	2.61 (0.02)	4.11 (0.05)	−5.9 (0.5)
	5	2.58 (0.01)	4.88 (0.03)	−5.1 (0.5)
K68M	0.85	2.71 (0.02)	4.29 (0.07)	−5.4 (0.5)
	5	2.81 (0.02)	5.08 (0.02)	−4.7 (0.5)
K68E	0.5	2.76 (0.02)	3.90 (0.08)	−5.2 (0.5)
	5	2.93 (0.02)	5.01 (0.04)	−4.5 (0.5)
E265Q	1	2.52 (0.02)	4.77 (0.05)	−6.3 (0.5)
	5	2.68 (0.02)	5.10 (0.05)	−5.4 (0.5)
E265K	0.85	2.23 (0.03)	4.59 (0.06)	−7.6 (0.4)
	5	2.31 (0.02)	5.27 (0.06)	−7.1 (0.4)
KMEQ	1	2.73 (0.01)	4.55 (0.04)	−5.3 (0.5)
	5	2.88 (0.02)	5.17 (0.02)	−4.6 (0.5)
KEEK	0.85	2.26 (0.09)	4.8 (0.7)	−6.7 (0.6)
	5	2.49 (0.02)	5.19 (0.08)	−6.5 (0.4)
R266K	2.5	2.8 (0.2)	4.50 (0.06)	−7.6 (1)
	10	2.82 (0.02)	5.14 (0.03)	−5.0 (0.5)
R266M	0.5	3.06 (0.02)	4.54 (0.04)	−3.8 (0.5)
	10	3.12 (0.01)	5.19 (0.02)	−3.4 (0.5)
N294D	0.5	3.86 (0.06)	4.9 (0.1)	0.0 (0.7)
	10	4.15 (0.06)	5.13(0.04)	0.8 (0.8)
N294R	10	3.30 (0.02)	5.17(0.04)	−2.6 (0.6)
N297R	0.5	2.91 (0.01)	4.24 (0.05)	−4.4 (0.5)
	10	2.66 (0.02)	5.47 (0.04)	−5.9 (0.5)

[a] All mutant $\Delta\Delta G^0_{D^*\rightleftarrows 2U}$ values are within experimental error of the one obtained for WT (see Figure 4). [b] $\Delta\Delta G^0$ values and standard errors were calculated from eqs 15−17.

to covary with the Lys68−Glu265* → Met68−Gln265* changes that differentiate plant mitochondria AATases from those from animal cytosolic and other organisms' AATases (*33*).

The free energy change for the interaction ($\Delta\Delta G^0_{int,D\rightleftarrows D^*}$) between Lys68 and Glu265* can be calculated from two double mutant cycles (*7, 45−47*), K68E ↔ E265K ↔ KEEK [$\Delta\Delta G^0_{int,D\rightleftarrows D^*(KEEK)} = -5.6 \pm 0.7$ kcal mol^{-1}] and K68M ↔ E265Q ↔ KMEQ [$\Delta\Delta G^0_{int,D\rightleftarrows D^*(KMEQ)} = -6 \pm 1$ kcal mol^{-1}] (Figure 5). The agreement between these two free energies of interaction indicates that the contacts of these two residues with their surroundings have little importance for the stability of eAATase. However, in terms of activity, $\Delta\Delta G^{\ddagger}_{int}$ values (calculated from k_{cat}/K_M parameters) are at least 2-fold larger for the K68E ↔ E265K ↔ KEEK double mutant cycle than for the K68M ↔ E265Q ↔ KMEQ double mutant cycle (*33*). Therefore, although the neighboring contacts of the Lys68−Glu265* pair are relatively important for maintaining the catalytic activity of the enzyme, they do not significantly contribute to its stability.

*(B) Asn294−Asn294**. Substitution with a larger positively charged residue at this site (N294R) results in a stronger destabilization effect than substitution with a nearly isosteric negatively charged replacement (N294D). The proximity of Arg113 to position 294 might explain why the N294R structure, which needs to accommodate an additional pair of bulky and positively charged side chains at this locus, results in a 2.5 ± 0.2 kcal mol^{-1} destabilization of D. In contrast, electrostatic interactions of N294D with Arg113

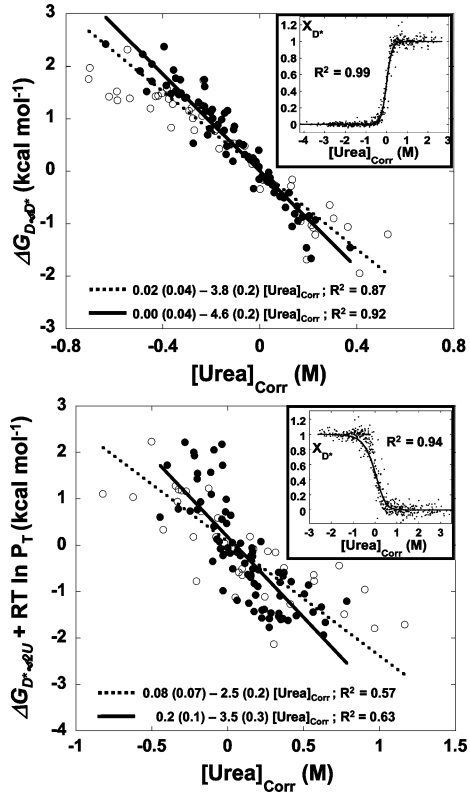

FIGURE 3: Determination of *m* values by linear extrapolation. $\Delta G_{D\rightleftarrows D^*}$ (top panel) and $\Delta G_{D^*\rightleftarrows 2U}$ (bottom panel) were calculated at each urea and enzyme concentration for all mutants (eqs 7−10). Black and white symbols represent denaturation conditions in which uncoupled and coupled transitions were observed, respectively. Corrected urea concentrations are $[\text{urea}]_{exp} - C_m$. Linear fits (eq 13 or 14) including (•••) or excluding (—) data from denaturation conditions resulting in overlapping transitions are shown. Insets show numerical fits of X_{D^*} vs $[\text{urea}]_{Corr}$ using the *m* values obtained from uncoupled transition data for the D ⇄ D* (top inset) and D* ⇄ 2U (bottom inset) equilibria.

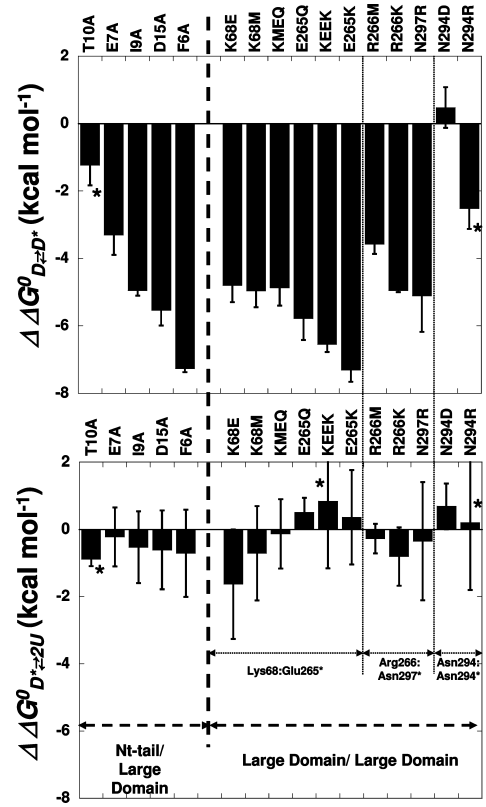

FIGURE 4: Effect of interface mutations on the stability of eAATase. $\Delta\Delta G^0_{D\rightleftarrows D^*}$ and $\Delta\Delta G^0_{D^*\rightleftarrows 2U}$ are shown in the top and bottom panels, respectively. Negative values indicate destabilizing effects. Mutants whose stabilities were measured at a single enzyme concentration are marked with asterisks.

and/or Arg113* may make this mutant as stable as WT [$\Delta\Delta G^0_{D\rightleftarrows D^*(N294D)} = 0.5 \pm 0.6$ kcal mol^{-1}]. However, this mutation results in a 100-fold decrease in $k_{cat}/K_{M,KG}$ (data not shown) despite the fact that Asn294 is situated >12 Å from the cofactor or substrate.

(C) Arg266−Asn297.* The guanidino group of Arg266 is in salt bridge contact with the phosphate moiety of PLP. Replacing Arg266 with a Lys is more detrimental than neutralizing the positive charge (R266M) (Table 2). This suggests that the opposite charges of the R266K amino group and of the cofactor's phosphate group do not interact productively. The N297R mutation buries two arginines in the proximity, resulting in a very unstable mutant.

The Nt Tail Is Crucial for Homodimer Stability. The two 11-amino acid Nt tails form extensive interactions with the backs of the large domains of the opposite subunits (*28*) (Figure 1). Met5, Phe6, and Ile9 interact with Val125*, Phe118*, and Val272*, all of which belong to a conserved hydrophobic cluster of ∼20 residues. A reduction in the size of this intersubunit surface (F6A and I9A) strongly decreases the stability of eAATase ($\Delta\Delta G^0_{D\rightleftarrows D^*} = -7.3 \pm 0.2$ and -5 ± 0.2 kcal mol^{-1}, respectively). Additionally, the salt bridge between the last residue of the Nt tail (Asp15) and the key substrate binding residue (Arg292*) contributes significantly to stability [$\Delta\Delta G^0_{D\rightleftarrows D^*(D15A)} = -5.4 \pm 0.2$ kcal mol^{-1}].

The importance of the internal structure of the Nt tail with respect to intersubunit interactions was investigated via the E7A and T10A mutants. The former breaks the interactions of the Glu7 carboxylate group with the amino terminus and the Met5−Phe6 peptide bond and results in a 3.3 ± 0.7 kcal mol^{-1} decrease in stability. The T10A mutation was expected to be inconsequential as it simply replaces the solvent-exposed hydroxyl group of Thr10 with a hydrogen atom, and only a modest decrease [$\Delta\Delta G^0_{D\rightleftarrows D^*(T10A)} = -1.2 \pm 0.2$ kcal mol^{-1}] was measured. These observations highlight the important role of the Nt tail with respect to the stability of eAATase. These results are in accord with those reported for other AATases such as that from *Bacillus circulans* (*51*) and the cytosolic (*52*) and mitochondrial (*53, 54*) isoenzymes where the importance of N-terminal regions was explored by complete or partial deletion as opposed to mutagenesis.

DISCUSSION

Multiple Interactions Contribute to Dimer Stability. Perturbation of each of the nine interactions shown in Table 1 results in destabilization of the native state by at least 1.2 ± 0.2 kcal mol^{-1}, independent of its location (large domain or Nt tail) or nature (salt bridge, hydrogen bond, or hydrophobic contact). The distribution of contributions to homodimer stability is more uniform than those of transient protein−protein complexes where a few key residues (hot spots) account for most of the free energies of association (*3−10, 12, 13*). The stability of the eAATase interface cannot be described as a sum of many weak interactions distributed across its large surface, as most positions tested could be

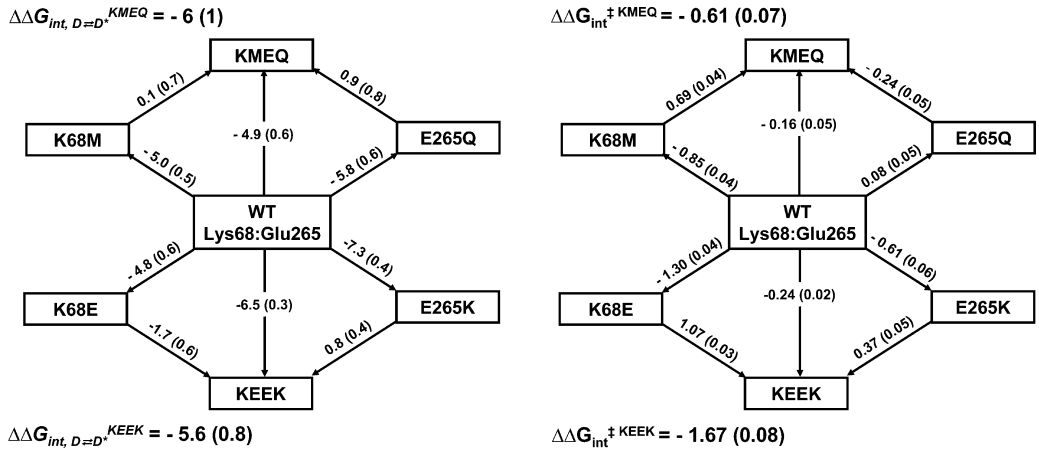

FIGURE 5: Double mutant cycle analysis of the contribution of the Lys68−Glu265* salt bridge to the stability (left) and activity (right) of eAATase. Charge to neutral and charge reversal mutations are shown in the top and bottom double mutant cycles, respectively. The values above each arrow correspond to $\Delta\Delta G^0_{D\rightleftarrows D^*}$ (Figure 4) and $\Delta\Delta G^{\ddagger}$. The latter were calculated from the $k_{cat}/K_{M,Asp}$ values reported in ref *33*. The free energies of interaction between Lys68 and Glu265* ($\Delta\Delta G_{int}$) are shown for each double mutant cycle. All free energy change values and their associated standard errors (in parentheses) are in kilocalories per mole.

defined as hot spots ($\Delta\Delta G^0_{D\rightleftarrows D^*} > 2$ kcal mol^{-1}) (*7*). Every mutation seems to perturb the interface globally as all variants unfold through the same denaturation pathway, i.e., D ⇄ D* ⇄ 2U. Contrary to what might be expected, none of the interface mutations perturbs the D* ⇄ 2U equilibrium. The residual stability of D* must therefore be provided through other interactions (see below).

Key Stabilizing Intersubunit Interactions Are Also Crucial for Catalysis. As each active site has components contributed by both monomers, the integrity of the homodimer is essential for catalytic activity. It is nonetheless interesting to note that important residues that are directly or indirectly involved in catalysis and cofactor binding are also important determinants of stability. These include Arg292 (*36*) and Asn297 (*37, 55, 56*), which are important for substrate specificity, Arg266 (*28, 30*), which helps to anchor the cofactor at the active site, Lys68 and Glu265, which are situated in the second shell of active site residues and tune the activity of eAATase (*33*), and the cofactor itself, which stabilizes the enzyme by >6 kcal mol^{-1} (*2*). Mutation of the remote Asn294 results in a substantial decrease in activity (J. Dhoot, unpublished data). Finally, deletion of the Nt tail in other AATase isoenzymes has been shown to impair these enzymes in terms of both catalysis and stability (*53, 57*). For example, sequential deletion of Nt residues in the *Pig* cytosolic isoenzyme results in increasingly compromised activities and thermostabilities (*52*).

Mutations at the D Interface Do Not Perturb the D* ⇄ 2U Equilibrium.* Several explanations might account for these observations. (1) The key intersubunit interactions responsible for the quaternary structure of D* were not selected for mutagenesis. Those might include some of the unperturbed contacts listed in Table 1 and/or interactions with the backbone. (2) The D and D* interfaces are not composed of the same set of residues. (3) The D* interface is very flexible and can accommodate single point mutations without observable effect on the stability of D* relative to U.

These explanations are not mutually exclusive. The results indicate that most native side chain−side chain intersubunit interactions become unstructured upon D* formation, which is accompanied by a 60% loss of secondary structure (*1*). In addition, PLP is unable to associate with D* (*2*). Therefore, an important structural perturbation of the dimeric interface takes place upon D* formation. On the other hand, D* is very stable relative to U ($\Delta G^0_{D^*\rightleftarrows 2U} = 25 \pm 1$ kcal mol^{-1}) and unfolds cooperatively ($m_{D^*\rightleftarrows 2U} = 3.5 \pm 0.3$ kcal mol^{-1} M^{-1}), which indicates the presence of significant tertiary structure. Overall, it is unlikely that the D ⇄ D* process would lead to the formation of a highly stable and structured interface involving a set of residues that is not found in the native interface. The sharpness of the D* ⇄ 2U transition is more likely due to the unfolding of residual tertiary structure nuclei inside the small and/or large domains rather than to the collapse of a newly formed interface in D*.

A possible structural model for the D* interface might be that of a nonrigid surface whose flexibility is mediated by the partial unfolding of the enzyme. Within that context, point mutations could be compensated locally through rearrangements of the backbone and side chain structures and by the shielding of repulsive electrostatic forces with water and urea molecules. The D* interface might thus be depicted as a "molten surface" whose disassembly is mediated by the unfolding of residual tertiary structure (Scheme 1).

The structural model depicted in Scheme 1 differs from that proposed in ref *2* in that the denatured region in D*

Scheme 1: Proposed Denaturation Model for eAATase in Urea[a]

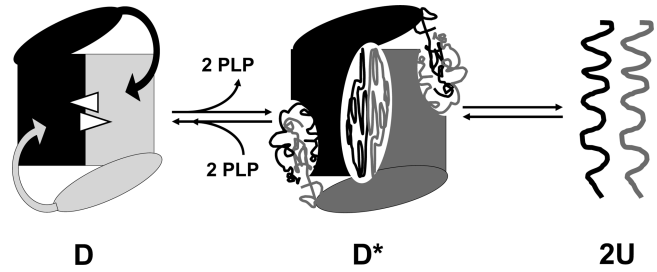

[a] Black and gray filled shapes represent the two subunits of the homodimer. Triangles, arrows, ovals, and rectangles represent the cofactors, Nt tails, and small and large domains, respectively. The "molten interface" described in the text for D* and the unfolded state are depicted by random coils, and the nuclei of the tertiary structure are contained in the still folded regions of the large and small domains. The illustrated extents of the unfolding of the polypeptide chain in D* are arbitrary.

extends throughout the interface and is not limited to the active site region. The previous model (*2*) was built exclusively on data obtained from the different WT forms, which differ only in the presence or absence of different cofactors in the active sites. The results presented above indicate that most side chain−side chain interactions are lost upon D* formation. Scheme 1 refines our previous model and includes this structural information by representing the full interface as a loosely packed molten surface.

An Unfolding Model for eAATase. All interface contacts involve interactions with the large domain, either between the two active site faces or through the Nt tails that wrap around them. Therefore, intersubunit perturbations would directly destabilize the large domain but not the small one, which does not form quaternary interactions. As reported in ref *2*, the D ⇄ D* transition accounts for >50% of the structural losses observed during unfolding and might correspond to the partial denaturation of the large domains into a molten globule-like structure. In that context, the D* interface might be held together through loose and/or indirect (mediated by water and urea molecules) interactions between the two partially folded large domains with themselves and/or with the Nt tails. In addition, the still folded small domain might provide a structured scaffold that stabilizes the D* quaternary structure (in D*, the small domain could also be directly involved in intersubunit interactions). Unfolding of the small domain would then result in monomer dissociation and explain the cooperative unfolding of the D* intermediate. The importance of the small domain with respect to the dimeric stability of the enzyme is evidenced by the fact that a truncated form of eAATase lacking the Nt tail and the small domain forms a folded monomeric protein (*58*), but deletion of only the Nt tail in several AATase isoenzymes is not sufficient to prevent dimerization (*52*−*54, 57*).

ACKNOWLEDGMENT

We thank Dr. Keith A. Koch for the cloning of His_6-tagged eAATase and its variants with mutations at positions 68, 265, and 266.

REFERENCES

1. Deu, E., and Kirsch, J. F. (2007) The Unfolding Pathway for Apo *E. coli* Aspartate Aminotransferase is Dependent on the Choice of Denaturant. *Biochemistry 46*, 5810–5818.
2. Deu, E., and Kirsch, J. F. (2007) Cofactor-directed Reversible Denaturation Pathways: The Cofactor-stabilized *E. coli* Aspartate Aminotransferase Homodimer Unfolds through a Pathway that Differs from that of the Apoenzyme. *Biochemistry 46*, 5819–5829.
3. Frisch, C., Fersht, A. R., and Schreiber, G. (2001) Experimental assignment of the structure of the transition state for the association of barnase and barstar. *J. Mol. Biol. 308*, 69–77.
4. Dalby, P. A., Clarke, J., Johnson, C. M., and Fersht, A. R. (1998) Folding intermediates of wild-type and mutants of barnase. II. Correlation of changes in equilibrium amide exchange kinetics with the population of the folding intermediate. *J. Mol. Biol. 276*, 647–656.
5. Dalby, P. A., Oliveberg, M., and Fersht, A. R. (1998) Folding intermediates of wild-type and mutants of barnase. I. Use of phi-value analysis and m-values to probe the cooperative nature of the folding pre-equilibrium. *J. Mol. Biol. 276*, 625–646.
6. Dalby, P. A., Oliveberg, M., and Fersht, A. R. (1998) Movement of the intermediate and rate determining transition state of barnase on the energy landscape with changing temperature. *Biochemistry 37*, 4674–4679.
7. Pons, J., Rajpal, A., and Kirsch, J. F. (1999) Energetic analysis of an antigen/antibody interface: Alanine scanning mutagenesis and double mutant cycles on the HyHEL-10/lysozyme interaction. *Protein Sci. 8*, 958–968.
8. Sundberg, E. J., and Mariuzza, R. A. (2002) Molecular recognition in antibody-antigen complexes. *Adv. Protein Chem. 61*, 119–160.
9. Pons, J., Stratton, J. R., and Kirsch, J. F. (2002) How do two unrelated antibodies, HyHEL-10 and F9.13.7, recognize the same epitope of hen egg-white lysozyme? *Protein Sci. 11*, 2308–2315.
10. Fuh, G., Wu, P., Liang, W. C., Ultsch, M., Lee, C. V., Moffat, B., and Wiesmann, C. (2006) Structure-function studies of two synthetic anti-vascular endothelial growth factor Fabs and comparison with the Avastin Fab. *J. Biol. Chem. 281*, 6625–6631.
11. Nickel, J., Dreyer, M. K., Kirsch, T., and Sebald, W. (2001) The crystal structure of the BMP-2:BMPR-IA complex and the generation of BMP-2 antagonists. *J. Bone Jt. Surg., Am. Vol. 83A* (Suppl. 1), S7–S14.
12. Duchesnes, C. E., Murphy, P. M., Williams, T. J., and Pease, J. E. (2006) Alanine scanning mutagenesis of the chemokine receptor CCR3 reveals distinct extracellular residues involved in recognition of the eotaxin family of chemokines. *Mol. Immunol. 43*, 1221–1231.
13. McFarland, B. J., Kortemme, T., Yu, S. F., Baker, D., and Strong, R. K. (2003) Symmetry recognizing asymmetry: Analysis of the interactions between the C-type lectin-like immunoreceptor NKG2D and MHC class I-like ligands. *Structure 11*, 411–422.
14. Zhang, J. L., Foster, D., and Sebald, W. (2003) Human IL-21 and IL-4 bind to partially overlapping epitopes of common gamma-chain. *Biochem. Biophys. Res. Commun. 300*, 291–296.
15. Inlow, J. K., and Baldwin, T. O. (2002) Mutational analysis of the subunit interface of *Vibrio harveyi* bacterial luciferase. *Biochemistry 41*, 3906–3915.
16. Grimsley, J. K., Scholtz, J. M., Pace, C. N., and Wild, J. R. (1997) Organophosphorus hydrolase is a remarkably stable enzyme that unfolds through a homodimeric intermediate. *Biochemistry 36*, 14366–14374.
17. Gloss, L. M., and Placek, B. J. (2002) The effect of salts on the stability of the H2A-H2B histone dimer. *Biochemistry 41*, 14951–14959.
18. Park, Y. C., and Bedouelle, H. (1998) Dimeric tyrosyl-tRNA synthetase from *Bacillus stearothermophilus* unfolds through a monomeric intermediate. A quantitative analysis under equilibrium conditions. *J. Biol. Chem. 273*, 18052–18059.
19. Yu, Y. B. (2002) Coiled-coils: Stability, specificity, and drug delivery potential. *Adv. Drug Delivery Rev. 54*, 1113–1129.
20. Mateu, M. G., Sanchez Del Pino, M. M., and Fersht, A. R. (1999) Mechanism of folding and assembly of a small tetrameric protein domain from tumor suppressor p53. *Nat. Struct. Biol. 6*, 191–198.
21. Sauer, R. T., Milla, M. E., Waldburger, C. D., Brown, B. M., and Schildbach, J. F. (1996) Sequence determinants of folding and stability for the P22 Arc repressor dimer. *FASEB J. 10*, 42–48.
22. Jaenicke, R. (1999) Stability and folding of domain proteins. *Prog. Biophys. Mol. Biol. 71*, 155–241.
23. Herold, M., and Kirschner, K. (1990) Reversible dissociation and unfolding of aspartate aminotransferase from *Escherichia coli*: Characterization of a monomeric intermediate. *Biochemistry 29*, 1907–1913.
24. Leistler, B., Herold, M., and Kirschner, K. (1992) Collapsed intermediates in the reconstitution of dimeric aspartate aminotransferase from *Escherichia coli*. *Eur. J. Biochem. 205*, 603–611.
25. Birolo, L., Malashkevich, V. N., Capitani, G., De Luca, F., Moretta, A., Jansonius, J. N., and Marino, G. (1999) Functional and structural analysis of cis-proline mutants of *Escherichia coli* aspartate aminotransferase. *Biochemistry 38*, 905–913.
26. Birolo, L., Dal Piaz, F., Pucci, P., and Marino, G. (2002) Structural characterization of the M* partly folded intermediate of wild type and P138A aspartate aminotransferase from *Escherichia coli*. *J. Biol. Chem. 277*, 17428–17437.
27. Gloss, L. M., Planas, A., and Kirsch, J. F. (1992) Contribution to catalysis and stability of the five cysteines in *Escherichia coli* aspartate aminotransferase. Preparation and properties of a cysteine-free enzyme. *Biochemistry 31*, 32–39.
28. Jager, J., Moser, M., Sauder, U., and Jansonius, J. N. (1994) Crystal structures of *Escherichia coli* aspartate aminotransferase in two conformations. Comparison of an unliganded open and two liganded closed forms. *J. Mol. Biol. 239*, 285–305.
29. Velick, S. F., and Vavra, J. (1962) A kinetic and equilibrium analysis of the glutamic oxaloacetate transaminase mechanism. *J. Biol. Chem. 237*, 2109–2122.
30. Kirsch, J. F., Eichele, G., Ford, G. C., Vincent, M. G., Jansonius, J. N., Gehring, H., and Christen, P. (1984) Mechanism of action

of aspartate aminotransferase proposed on the basis of its spatial structure. *J. Mol. Biol. 174*, 497–525.
31. Eliot, A. C., and Kirsch, J. F. (2004) Pyridoxal phosphate enzymes: Mechanistic, structural, and evolutionary considerations. *Annu. Rev. Biochem. 73*, 383–415.
32. Goldberg, J. M., and Kirsch, J. F. (1996) The reaction catalyzed by *Escherichia coli* aspartate aminotransferase has multiple partially rate-determining steps, while that catalyzed by the Y225F mutant is dominated by ketimine hydrolysis. *Biochemistry 35*, 5280–5291.
33. Deu, E., Koch, K. A., and Kirsch, J. F. (2002) The role of the conserved Lys68*:Glu265 intersubunit salt bridge in aspartate aminotransferase kinetics: Multiple forced covariant amino acid substitutions in natural variants. *Protein Sci. 11*, 1062–1073.
34. Toney, M. D., and Kirsch, J. F. (1991) Kinetics and equilibria for the reactions of coenzymes with wild type and the Y70F mutant of *Escherichia coli* aspartate aminotransferase. *Biochemistry 30*, 7461–7466.
35. Toney, M. D., and Kirsch, J. F. (1991) Tyrosine 70 fine-tunes the catalytic efficiency of aspartate aminotransferase. *Biochemistry 30*, 7456–7461.
36. Cronin, C. N., and Kirsch, J. F. (1988) Role of arginine-292 in the substrate specificity of aspartate aminotransferase as examined by site-directed mutagenesis. *Biochemistry 27*, 4572–4579.
37. Onuffer, J. J., and Kirsch, J. F. (1995) Redesign of the substrate specificity of *Escherichia coli* aspartate aminotransferase to that of *Escherichia coli* tyrosine aminotransferase by homology modeling and site-directed mutagenesis. *Protein Sci. 4*, 1750–1757.
38. Nozaki, Y. (1972) The preparation of guanidine hydrochloride. *Methods Enzymol. 26* (Part C), 43–50.
39. Pace, C. N. (1986) Determination and analysis of urea and guanidine hydrochloride denaturation curves. *Methods Enzymol. 131*, 266–280.
40. Santoro, M. M., and Bolen, D. W. (1988) Unfolding free energy changes determined by the linear extrapolation method. 1. Unfolding of phenylmethanesulfonyl α-chymotrypsin using different denaturants. *Biochemistry 27*, 8063–8068.
41. Barrick, D., and Baldwin, R. L. (1993) Three-state analysis of sperm whale apomyoglobin folding. *Biochemistry 32*, 3790–3796.
42. Pace, C. N., and Shaw, K. L. (2000) Linear extrapolation method of analyzing solvent denaturation curves. *Proteins Suppl. 4*, 1–7.
43. Clark, A. C., Sinclair, J. F., and Baldwin, T. O. (1993) Folding of bacterial luciferase involves a non-native heterodimeric intermediate in equilibrium with the native enzyme and the unfolded subunits. *J. Biol. Chem. 268*, 10773–10779.
44. Clarke, J., and Fersht, A. R. (1993) Engineered disulfide bonds as probes of the folding pathway of barnase: Increasing the stability of proteins against the rate of denaturation. *Biochemistry 32*, 4322–4329.
45. Ackers, G. K., and Smith, F. R. (1985) Effects of site-specific amino acid modification on protein interactions and biological function. *Annu. Rev. Biochem. 54*, 597–629.
46. Horovitz, A. (1987) Non-additivity in protein-protein interactions. *J. Mol. Biol. 196*, 733–735.
47. Horovitz, A. (1996) Double-mutant cycles: A powerful tool for analyzing protein structure and function. *Folding Des. 1*, R121−R126.
48. Reyes, A. M., Iriarte, A., and Martinez-Carrion, M. (1993) Refolding of the precursor and mature forms of mitochondrial aspartate aminotransferase after guanidine hydrochloride denaturation. *J. Biol. Chem. 268*, 22281–22291.
49. Myers, J. K., Pace, C. N., and Scholtz, J. M. (1995) Denaturant m values and heat capacity changes: Relation to changes in accessible surface areas of protein unfolding. *Protein Sci. 4*, 2138–2148.
50. Spudich, G., and Marqusee, S. (2000) A change in the apparent m value reveals a populated intermediate under equilibrium conditions in *Escherichia coli* ribonuclease HI. *Biochemistry 39*, 11677–11683.
51. Kravchuk, Z., Tsybovsky, Y., Koivulehto, M., Vlasov, A., Chumanevich, A., Battchikova, N., Martsev, S., and Korpela, T. (2001) Truncated aspartate aminotransferase from alkalophilic *Bacillus circulans* with deletion of N-terminal 32 amino acids is a nonfunctional monomer in a partially structured state. *Protein Eng. 14*, 279–285.
52. Fukumoto, Y., Tanase, S., Nagashima, F., Ueda, S., Ikegami, K., and Morino, Y. (1991) Structural and functional role of the amino-terminal region of porcine cytosolic aspartate aminotransferase. Catalytic and structural properties of enzyme derivatives truncated on the amino-terminal side. *J. Biol. Chem. 266*, 4187–4193.
53. Sandmeier, E., and Christen, P. (1980) Mitochondrial aspartate aminotransferase 27/32-410. Partially active enzyme derivative produced by limited proteolytic cleavage of native enzyme. *J. Biol. Chem. 255*, 10284–10289.
54. Iriarte, A., Hubert, E., Kraft, K., and Martinez-Carrion, M. (1984) Selective tryptic cleavage of native cytoplasmic aspartate transaminase holoenzyme. *J. Biol. Chem. 259*, 723–728.
55. Rothman, S. C., and Kirsch, J. F. (2003) How does an enzyme evolved in vitro compare to naturally occurring homologs possessing the targeted function? Tyrosine aminotransferase from aspartate aminotransferase. *J. Mol. Biol. 327*, 593–608.
56. Shaffer, W. A., Luong, T. N., Rothman, S. C., and Kirsch, J. F. (2002) Quantitative chimeric analysis of six specificity determinants that differentiate *Escherichia coli* aspartate from tyrosine aminotransferase. *Protein Sci. 11*, 2848–2859.
57. Azzariti, A., Vacca, R. A., Giannattasio, S., Merafina, R. S., Marra, E., and Doonan, S. (1998) Kinetic properties and thermal stabilities of mutant forms of mitochondrial aspartate aminotransferase. *Biochim. Biophys. Acta 1386*, 29–38.
58. Herold, M., Leistler, B., Hage, A., Luger, K., and Kirschner, K. (1991) Autonomous folding and coenzyme binding of the excised pyridoxal 5′-phosphate binding domain of aspartate aminotransferase from *Escherichia coli*. *Biochemistry 30*, 3612–3620.

BI801431X